Physics Letters B 672 (2009) 22–29

Contents lists available at ScienceDirect

Physics Letters B

www.elsevier.com/locate/physletb

The ^{8}He and ^{10}He spectra studied in the (t, p) reaction

M.S. Golovkov [a], L.V. Grigorenko [a,b,c], G.M. Ter-Akopian [a,*], A.S. Fomichev [a], Yu.Ts. Oganessian [a], V.A. Gorshkov [a], S.A. Krupko [a], A.M. Rodin [a], S.I. Sidorchuk [a], R.S. Slepnev [a], S.V. Stepantsov [a], R. Wolski [a,d], D.Y. Pang [a,e], V. Chudoba [a,f], A.A. Korsheninnikov [c], E.A. Kuzmin [c], E.Yu. Nikolskii [c,g], B.G. Novatskii [c], D.N. Stepanov [c], P. Roussel-Chomaz [h], W. Mittig [h], A. Ninane [i], F. Hanappe [j], L. Stuttgé [k], A.A. Yukhimchuk [l], V.V. Perevozchikov [l], Yu.I. Vinogradov [l], S.K. Grishechkin [l], S.V. Zlatoustovskiy [l]

[a] *Flerov Laboratory of Nuclear Reactions, JINR, RU-141980 Dubna, Russia*
[b] *Gesellschaft für Schwerionenforschung mbH, Planckstrasse 1, D-64291 Darmstadt, Germany*
[c] *Russian Research Center "The Kurchatov Institute", Kurchatov sq. 1, RU-123182 Moscow, Russia*
[d] *Henryk Niewodniczanski Institute of Nuclear Physics, Cracow, Poland*
[e] *Department of Technical Physics, Peking University, 100871 Beijing, People's Republic of China*
[f] *Faculty of Nuclear Sciences and Physical Engineering, Czech Technical University, 11519 Prague, Czech Republic*
[g] *RIKEN, Hirosawa 2-1, Wako, Saitama 351-0198, Japan*
[h] *GANIL, BP 5027, F-14076 Caen Cedex 5, France*
[i] *Slashdev Integrated Systems Solutions, Rue de la Rochette, 26, B-5030 Gembloux, Belgium*
[j] *Université Libre de Bruxelles, PNTPM, Bruxelles, Belgium*
[k] *Institut de Recherches Subatomiques, IN2P3/Université Louis Pasteur, Strasbourg, France*
[l] *RNFC – All-Russian Research Institute of Experimental Physics, RU-607190 Sarov, Nizhni Novgorod Region, Russia*

ARTICLE INFO

Article history:
Received 27 March 2008
Received in revised form 11 July 2008
Accepted 19 December 2008
Available online 31 December 2008
Editor: V. Metag

PACS:
25.10.+s
24.50.+g
25.55.Hp
25.60.Je
21.60.Gx

Keywords:
^{6}He
^{8}He beams
Tritium gas target
Resonance states
Hyperspherical harmonic method
Soft dipole mode
Neutron halo

ABSTRACT

The low-lying spectra of ^{8}He and ^{10}He nuclei were studied in the ^{3}H(^{6}He, p)^{8}He and ^{3}H(^{8}He, p)^{10}He transfer reactions. The 0^{+} ground state (g.s.) of ^{8}He and excited states, 2^{+} at 3.6–3.9 MeV and (1^{+}) at 5.3–5.5 MeV, were populated with cross sections of 200, 100–250, and 90–125 μb/sr, respectively. Some evidence for a ^{8}He state at about 7.5 MeV was obtained. We discuss a possible nature of the near-threshold anomaly above 2.14 MeV in ^{8}He and relate it to the population of a 1^{-} continuum (soft dipole excitation) with a peak value at about 3 MeV. The lowest energy group of events in the ^{10}He spectrum was observed at ~ 3 MeV with a cross section of ~ 140 μb/sr. We argue that this result is consistent with the previously reported observation of ^{10}He providing the new ^{10}He g.s. position at about 3 MeV.

1. Introduction

To study drip-line nuclei with large neutron excess one should either transfer neutrons or remove protons or make multi-nucleon charge-exchange. Two-neutron transfer from tritium provides here important opportunities connected with the simplicity of the reaction mechanism and the simplicity of the recoil particle (proton) registration. This class of reactions remains practically not exploited in the radioactive beam research. The unique cryogenic tritium target [1] available at the Flerov Laboratory of Nuclear Reactions (JINR, Dubna) makes possible systematic studies of these reactions. The effectiveness of such an approach in the investigation of exotic nuclei was demonstrated in the recent studies of the ^{5}H system [2,3].

* Corresponding author.
E-mail address: gurgen.terakopian@jinr.ru (G.M. Ter-Akopian).

0370-2693/$ – see front matter
doi:10.1016/j.physletb.2008.12.052

Although ^{10}He has been experimentally discovered more than a decade ago [4], very limited information on this system is available. The ground state properties were found in the ^{2}H(^{11}Li, ^{10}He)X reaction as $E_{^{10}\mathrm{He}} = 1.2(3)$, $\Gamma < 1.2$ MeV [4], and in the ^{10}Be(^{14}C, ^{14}O)^{10}He reaction as $E_{^{10}\mathrm{He}} = 1.07(7)$, $\Gamma = 0.3(2)$ MeV [5,6]. Here and below $E_{A\mathrm{He}}$ denotes the energy relative to the lowest breakup threshold for the $A = \{6, 8, 10\}$ systems, while E denotes the excitation energy.

As for the theoretical studies, the ^{10}He g.s. was predicted in Ref. [7] to be a narrow three-body $^{8}\mathrm{He} + n + n$ resonance with $E_{^{10}\mathrm{He}} \sim 0.7$–$0.9$ MeV, $\Gamma \sim 0.1$–0.3 MeV, and the valence neutrons populating mainly the $[p_{1/2}]^2$ configuration. The widely discussed shell inversion phenomenon in the $N = 7$ nuclei became the source of a new interest to ^{10}He. The possible existence of a virtual state in ^{9}He was demonstrated in Ref. [8], and an *upper* limit $a < -10$ fm was established for the scattering length. Following this finding, the existence of a narrow near-threshold 0^+ state in ^{10}He ($E_{^{10}\mathrm{He}} = 0.05$, $\Gamma = 0.21$ MeV) with the $[s_{1/2}]^2$ structure was predicted in Ref. [9] in addition to the $[p_{1/2}]^2$ 0^+ state. It was suggested in [9] that the ground state of ^{10}He had not been observed so far, and the resonance at ~ 1.2 MeV is actually the first excited state. The low-lying spectrum of ^{9}He was revised in the recent experiment [10] resulting in a higher, than in the previous studies, position of the $p_{1/2}$ state (experiment [10] provided a unique spin-parity identification for the ^{9}He states below 5 MeV). The presence of a $s_{1/2}$ contribution is evident in the data [10], but the exact nature of this contribution (virtual state or nonresonant s-wave continuum) was not clarified, and only a *lower* limit $a > -20$ fm was set in this work. This work triggered further theoretical research: problems with the interpretation of the ^{10}He spectrum and the controversy between the ^{9}He and ^{10}He data were demonstrated in Ref. [11].

This intriguing situation inspired us to revisit the ^{10}He issue. The study of the ^{3}H(^{8}He, p)^{10}He reaction was accompanied by the study of the ^{3}H(^{6}He, p)^{8}He reaction providing for a reference case of the relatively well investigated ^{8}He system.

2. Experimental setup

Experiments were performed using a 34 MeV/amu primary beam of ^{11}B delivered by the JINR U-400M cyclotron. The secondary beams of the ^{6}He and ^{8}He nuclei were produced by the separator ACCULINNA [12] and focused in a 20 mm spot on the target cell. For safety reasons, the main target cell, filled with the 900 mPa tritium gas and cooled down to 28 K, was inserted into the evacuated protective box. Thus, the target had twin entrance and exit windows sealed with 12.7 μm stainless steel foils. For a 4 mm distance between the inner entrance and exit windows the thickness of the tritium target was 2.0×10^{20} cm^{-2}. Typical beam intensities were $\sim 4 \times 10^{4}$ s^{-1} for the ^{6}He and $\sim 6 \times 10^{3}$ s^{-1} for the ^{8}He projectile nuclei. The beam contaminations were no more than 7%; the beam diagnostics system completely eliminated their effect. For the ^{6}He and ^{8}He beams the projectile energies in the middle of the tritium target were on average about 25 MeV/amu and 27.4 MeV/amu, respectively; current integrals of 2×10^{10} and 5×10^{9} were collected.

Experimental setup and kinematical diagram for the ^{3}H(^{6}He, p)^{8}He and ^{3}H(^{8}He, p)^{10}He reactions are shown in Fig. 1. For the small centre-of-mass system (CMS) angles, where the maximal cross sections are expected, the protons fly in the backward direction in the lab system. The residuals (^{10}He and ^{8}He) and their decay products (^{8}He and ^{6}He) move in a relatively narrow angular cone in the forward direction. Protons emitted to the backward hemisphere were detected by the telescope consisting of one 300 μm and one 1 mm thick annular Si detectors. The active areas of these detectors had the outer and inner diameters

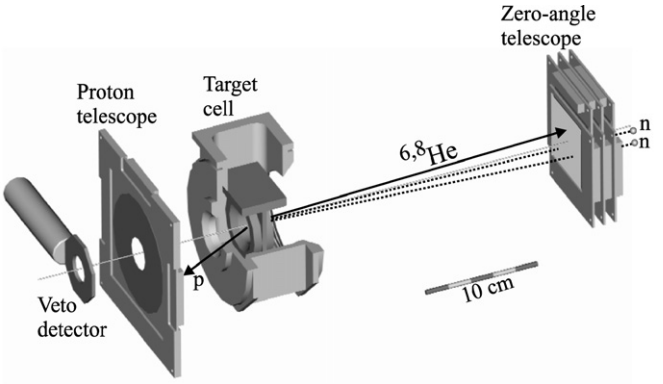

Fig. 1. Experimental setup and kinematical diagram.

of 82 mm and 32 mm, respectively. The proton telescope was installed 100 mm upstream of the target and covered an angular range of 171°–159° in lab system. The first detector was segmented in 16 rings on one side and 16 sectors on the other side and the second, 1 mm detector was not segmented. A veto detector was installed upstream of the proton telescope to alert to the signals generated by the beam halo.

Zero angle telescope for the ^{6}He and ^{8}He detection was installed on the beam axis at a distance of 36.5 cm in the case of the ^{6}He beam and at 28.8 cm in the experiment with the ^{8}He beam. The telescope included six squared (60×60 mm) 1 mm thick detectors. The first two detectors of the telescope were segmented in 16 strips each in vertical and horizontal directions. All other detectors in the telescope were segmented in 4 strips in the ^{8}He run and in 16 strips in the ^{6}He run.

A set of beam detectors was installed upstream of the veto detector (not shown in Fig. 1). Two 0.5 mm plastic scintillators placed on a 8 m base provided the particle identification and projectile energy measurement. The overall time resolution was 0.5 ns. The beam tracking, giving a 1.5 mm resolution for the target hit position, was made using two multiwire chambers installed 26 and 80 cm upstream of the target.

Particle identification in the proton telescope was not imperative because, due to kinematical constraints, nothing but protons could be emitted in the backward direction in these reactions. The main background originated from the interactions of beam nuclei with the target windows. Test runs performed with the empty target showed that this background was almost completely eliminated for the p–^{6}He coincidences (see Fig. 2) and completely eliminated for the p–^{8}He coincidences. In the case of the ^{3}H(^{6}He, p)^{8}He reaction the detection of the p–^{8}He coincidence events granted selection for the reaction channel populating the ^{8}He g.s. For the decays of ^{10}He and excited ^{8}He nuclei the respective p–^{8}He and p–^{6}He coincidence information was used to clean the missing mass spectra and reconstruct the charged fragment energy in the CMS of ^{10}He or ^{8}He.

Array of 48 detector modules of the neutron time-of-flight spectrometer DEMON [13] was installed in the forward direction at a distance of 3.1 m from the target. In more rare events where the triple p–^{6}He–n coincidences were detected the complete reaction kinematics was reconstructed.

The missing mass spectrum of ^{8}He was measured up to 14 MeV of excitation energy; the ^{10}He spectrum was measured up to 16 MeV above the $^{8}\mathrm{He} + n + n$ threshold. These limits were conditioned by the 1.8 MeV low-energy threshold set for the proton detection. Monte Carlo (MC) simulations taking into account the details of these experiments showed that a 450 keV (FWHM) resolution was inherent to the ^{8}He and ^{10}He missing mass energy spectra obtained from the data. The precision of the beam energy

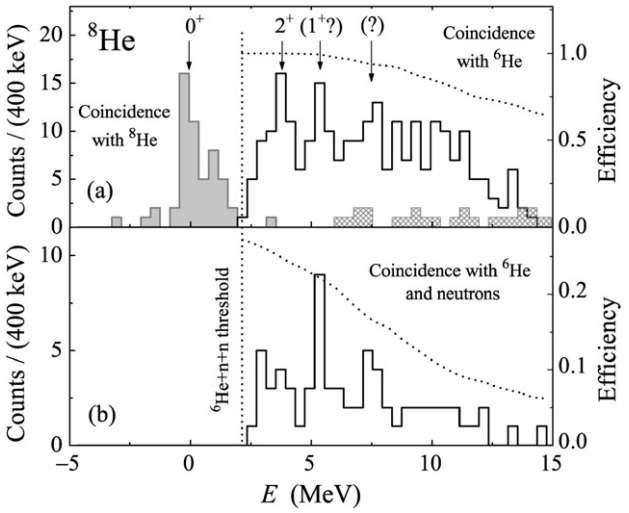

Fig. 2. Missing mass spectrum of ^{8}He. (a) The p–^{8}He and p–^{6}He coincidence data were used to obtain the ground state peak and the excited state spectrum, respectively. The hatched histogram demonstrates the measured background contribution: the empty target run results are shown, processed in the same way as the real data and scaled to the beam current integral of the working run. (b) Spectrum built for the ^{8}He excited states from the p–^{6}He–n coincidence data. The efficiencies of the p–^{6}He and p–^{6}He–n coincidence registration are shown by dotted curves (see the right axes in both panels).

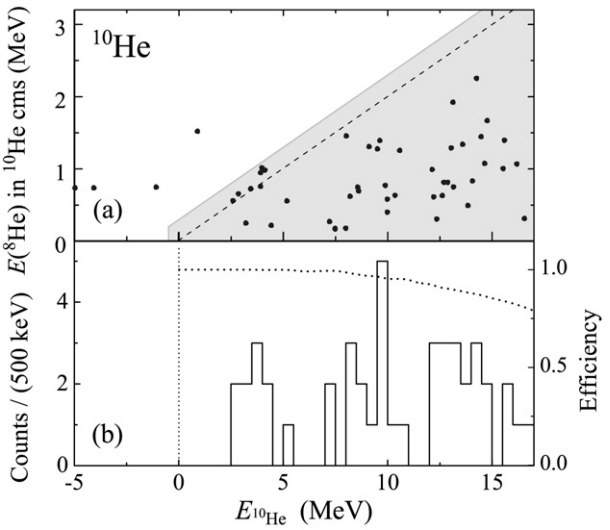

Fig. 3. Scatter plot showing the ^{8}He energy observed in the ^{10}He CMS frame versus the ^{10}He missing mass energy. (b) Missing mass spectrum of ^{10}He. The p–^{8}He coincidence efficiency is shown by dotted curve (see right axis).

measurement made the most important contribution to the derived missing mass uncertainty.

3. ^{3}H(^{6}He, p)^{8}He reaction

Missing mass spectra of ^{8}He from the ^{3}H(^{6}He, p)^{8}He reaction are presented in Fig. 2. The peak corresponding to the ^{8}He g.s. is evident in the p–^{8}He coincidence data. The tail visible in Fig. 2(a) on the right side of the g.s. peak was caused by the pile-ups in the second (non-segmented) detector. The protons emitted from the target with energy ~ 8.5 MeV correspond to the population of the ^{8}He ground state. They passed through the 300 μm Si detector and stopped in the second (1 mm) detector of the proton telescope. The background signals arose here from the beam halo particles [count rate of $(2\text{–}3) \times 10^3$ s^{-1}]. The veto detector allowed taking away these events in the data analysis but the energy resolution of the second detector was deteriorated. Operation conditions were much better for the segmented 300 μm detector. The count rate per any of its sectors was at least 10 times lower. Consequently, the background signals did not cause the resolution deterioration when the p–^{6}He coincidences were detected. In that case protons with energy < 7.5 MeV were emitted from the target and practically all of them were stopped in the 300 μm detector. Therefore, for the ^{8}He excited states the stated 450 keV resolution is valid.

There are two peaks apparent in the ^{8}He excitation spectrum. We assign 2^+ to the ^{8}He resonance at the excitation energy $E \approx 3.6$ MeV. The 2^+ resonance with energy 3.57 ± 0.12 MeV and width $\Gamma = 0.5 \pm 0.35$ MeV was for the first time unambiguously, and with that good precision, obtained in Ref. [14]. Later on, this resonance was reported in a number of papers with energies close to 3.6 MeV and widths $\Gamma \approx 0.5\text{–}0.8$ MeV (see, e.g., [6,15,16] and references therein). We assume that the $E \approx 5.4$ MeV peak seen in Fig. 2 is the 1^+ resonance of ^{8}He. The ground for this assumption comes from various theoretical results (e.g. [17–19]) stably predicting that in the ^{8}He excitation spectrum the next state after the 2^+ should be the 1^+ state. We note that the evidence for the peak at $E \sim 5\text{–}6$ MeV was found in Ref. [14]. The ^{8}He excited state at 5.4 MeV was recently reported also in Ref. [16]. A rapid rise of the ^{8}He spectrum at the $^6\text{He} + n + n$ decay threshold is seen in Fig. 2. This rise cannot be explained by the left "wing" of the 2^+ resonance. The peculiar threshold behaviour is discussed in Section 6. We note also that the spectra in Fig. 2 show some evidence for a ^{8}He state at $E \approx 7.5$ MeV.

In the ^{3}H(^{6}He, p)^{8}He reaction the population cross section for the ^{8}He g.s., averaged in a range of 4°–10° of the reaction CMS, is found to be ~ 200 μb/sr. The observed threshold anomaly makes the cross section derivation for the excited states of ^{8}He more complicated (and model dependent). The cross sections for the excited states are further discussed in Sections 5 and 6.

4. ^{3}H(^{8}He, p)^{10}He reaction

Data obtained for the ^{3}H(^{8}He, p)^{10}He reaction are shown in Fig. 3(a) as a scatter plot $E(^8\text{He})$ vs. $E_{^{10}\text{He}}$, where $E(^8\text{He})$ is the energy of ^{8}He in the ^{10}He CMS. Condition $5E(^8\text{He}) \leqslant E_{^{10}\text{He}}$ should be valid for the ^{10}He decay. Therefore, ^{10}He events should be below the boundary shown by the dashed line in the scatter plot of Fig. 3(a). The shaded area in Fig. 3(a) extends this boundary accounting for the experimental resolution. One can see that practically all the events presented in Fig. 3(a) fall into the ^{10}He locus indicating very clean background conditions. The missing mass spectrum in Fig. 3(b) was obtained by projecting the events confined in the ^{10}He locus.

Not a single event was detected in the ^{10}He spectrum below 2.5 MeV. This imposes a stringent limit (one count corresponds to 14 μb/sr) on the population cross section in the expected ^{10}He ground state region at about 1.2 MeV [4]. The lowest energy feature in the ^{10}He spectrum is a group of 10 events in between 2.5 and 5.5 MeV [see Fig. 3]. This ~ 3 MeV group is well isolated from the rest of the spectrum and has a typical resonant cross section (~ 140 μb/sr averaged for CMS angles 3.5°–9.5°), see estimates in Section 5. Also, this group has a distinct feature: the energy distribution of the ^{8}He fragments obtained in the ^{10}He CMS appears to be different from that for the rest of events in the ^{10}He spectrum. One can see in Fig. 3(a) that within this group the $E(^8\text{He})$ energies concentrate around the maximal possible value. This means that the relative energy of the decay neutrons for such events tends to be zero. This could be evidence for some strong specific momentum correlations or/and strong n–n final state interaction in this part of the ^{10}He spectrum. We think that the ~ 3 MeV group of events represents a resonant state for ^{10}He. This assumption is jus-

tified by the cross section estimates of Section 5; a possible nature of this state is discussed in Section 7.

5. Cross section estimates

Both the ^{8}He and ^{10}He states were populated in our experiments by the same "dineutron" transfer in the same kinematical conditions and, presumably, by the same direct reaction mechanism. This makes it very probable that spectroscopic information can be extracted from the cross sections in a straightforward way. For theoretical estimates of the spectroscopic factors we used a somewhat extended phenomenological Cluster Oscillator Shell Model Approximation (COSMA) of Ref. [20]. Within this model the g.s. wave functions (WF) Ψ^J of the ^{6,8,10}He isotopes can be written as

$$\Psi^0_{^6\mathrm{He}} = \alpha_6\big[p^2_{3/2}\big]_0 + \beta_6\big[p^2_{1/2}\big]_0,$$
$$\Psi^0_{^8\mathrm{He}} = \alpha_8\big[p^4_{3/2}\big]_0 + \beta_8\big[p^2_{3/2}p^2_{1/2}\big]_0,$$
$$\Psi^{0(p)}_{^{10}\mathrm{He}} = \big[p^4_{3/2}p^2_{1/2}\big]_0, \qquad \Psi^{0(s)}_{^{10}\mathrm{He}} = \big[p^4_{3/2}s^2_{1/2}\big]_0. \tag{1}$$

Schematic notation $[l^n_j]_J$ denotes the Slater determinant of n neutrons occupying l_j orbital projected on the total spin J and normalized. The α-particle is considered to be an inert core and it is omitted in the notation. In the original paper [20] only the α_8 configuration in Eq. (1) was considered. For ^{10}He we consider separately the WFs with $[p_{1/2}]^2$ and $[s_{1/2}]^2$ configurations of the last valence nucleons.

The model looks very schematic. However, it lists *all* the possible p-shell configurations representing the dominant part of the WF. Particularly, for the ^{6}He g.s. coefficients α_6, β_6 can be inferred from the three-cluster model calculations [21]

$$\alpha_6 = 0.926, \qquad \alpha_6^2 = 0.86, \qquad \beta_6 = 0.226, \qquad \beta_6^2 = 0.05,$$

exhausting 91% of the WF normalization (the corresponding 79% of $K=2$, $L=0$ and 12% of $K=2$, $L=1$ components are considered). The simplified ^{6}He WF can also be used with only $p_{3/2}$ configuration ($\alpha_6 = 1$, $\beta_6 = 0$) to test the sensitivity to the ^{6}He structure. Assuming that the ^{8}He WF (1) is normalized, we end up with only one unknown parameter β_8 in the model.

The cluster overlaps for the ^{8,10}He WFs within this model are:

$$\big\langle \Psi^0_{^8\mathrm{He}} \big| \Psi^0_{^6\mathrm{He}} \big\rangle = \frac{\alpha_6\beta_8}{\sqrt{6}}\big[p^2_{1/2}\big]_0 + \frac{\beta_6\beta_8 - \alpha_6\sqrt{1-\beta_8^2}}{\sqrt{6}}\big[p^2_{3/2}\big]_0,$$
$$\big\langle \Psi^{0(p)}_{^{10}\mathrm{He}} \big| \Psi^0_{^8\mathrm{He}} \big\rangle = \frac{\sqrt{1-\beta_8^2}}{\sqrt{15}}\big[p^2_{1/2}\big]_0 - \frac{\beta_8}{\sqrt{15}}\big[p^2_{3/2}\big]_0,$$
$$\big\langle \Psi^{0(s)}_{^{10}\mathrm{He}} \big| \Psi^0_{^8\mathrm{He}} \big\rangle = \frac{\sqrt{1-\beta_8^2}}{\sqrt{15}}\big[s^2_{1/2}\big]_0. \tag{2}$$

Using spin algebra and Talmi coefficients, the overlaps of the shell model configurations with the "dineutron" nn being in the s-wave motion relative to the core are obtained as

$$\big\langle \big[p^2_{3/2}\big]_0 | nn \big\rangle = \sqrt{\frac{2}{6}}, \qquad \big\langle \big[p^2_{1/2}\big]_0 | nn \big\rangle = \sqrt{\frac{1}{6}}, \qquad \big\langle \big[s^2_{1/2}\big]_0 | nn \big\rangle = 1.$$

"Dineutron" here is the two neutrons with angular momentum and total spin equal to zero represented by the minimal oscillator. The spectroscopic weight of the ^{6}He g.s. configuration in the ^{8}He WF is obtained by Eq. (2) as

$$\big\| \big\langle \Psi^0_{^8\mathrm{He}} \big| \Psi^0_{^6\mathrm{He}} \big\rangle \big\| = \frac{1}{6}\big[\alpha_6^2\beta_8^2 + \big(\beta_6\beta_8 - \alpha_6\sqrt{1-\beta_8^2}\big)^2\big]. \tag{3}$$

For the reactions studied in this work a reasonable estimate of the cross section ratio σ_{10}/σ_8 for the ^{10}He and ^{8}He g.s. population is the ratio of the dineutron spectroscopic factors. They are found as

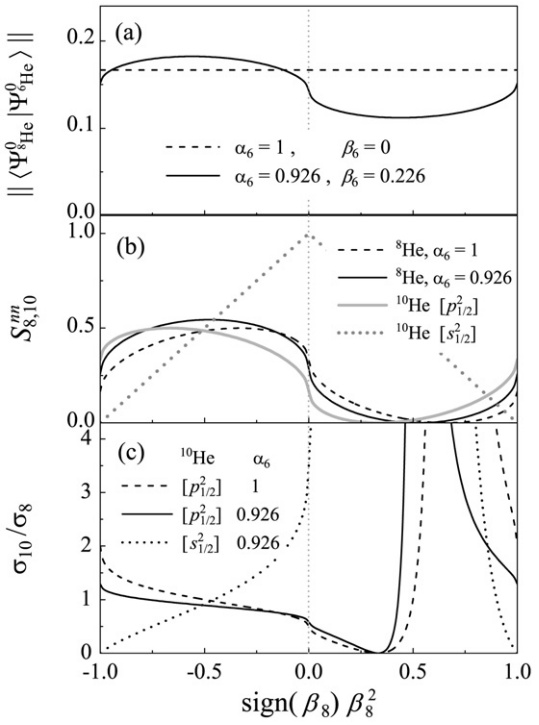

Fig. 4. (a) Spectroscopic weight (3) of the ^{6}He g.s. configuration in ^{8}He WF for the simplified ($\alpha_6 = 1$) and realistic structures of ^{6}He. (b) Two-neutron spectroscopic factors in ^{8}He and ^{10}He. (c) Estimated cross section ratio for the ^{10}He and ^{8}He g.s. population in the (t, p) reaction.

$$S^{nn}_8 = \frac{4!}{2!2!}\big\langle \Psi^0_{^8\mathrm{He}} \big| \Psi^0_{^6\mathrm{He}}, nn \big\rangle^2 = \frac{1}{6}\big[\alpha_6\big(\beta_8 - \sqrt{2(1-\beta_8^2)}\big) + \sqrt{2}\beta_6\beta_8\big]^2,$$
$$S^{nn}_{10}(p) = \frac{6!}{2!4!}\big\langle \Psi^{0(p)}_{^{10}\mathrm{He}} \big| \Psi^0_{^8\mathrm{He}}, nn \big\rangle^2 = \frac{1}{6}\big[\sqrt{1-\beta_8^2} - \sqrt{2}\beta_8\big]^2,$$
$$S^{nn}_{10}(s) = \frac{6!}{2!4!}\big\langle \Psi^{0(s)}_{^{10}\mathrm{He}} \big| \Psi^0_{^8\mathrm{He}}, nn \big\rangle^2 = 1 - \beta_8^2.$$

The spectroscopic information obtained in the model is illustrated in Fig. 4. In the region $\beta_8 > 0$ the cross section ratio is changing dramatically [Fig. 4(c)]. However, this region is presumably unphysical. In this region the weight of the dineutron configuration in ^{8,10}He is minimal [Fig. 4(b)] and the weight of the ^{6}He g.s. configuration in ^{8}He is minimal as well [Fig. 4(a)]. These configurations are expected to be maximized by the variational procedure as they are energetically highly preferable. Simple heuristic considerations show that the β_8 coefficient should be confined by the conditions $\beta_8 < 0$ [to maximize the attractive (ls) interaction] and $-0.5 < \mathrm{sign}(\beta_8)\beta_8^2 < -0.3$ [to maximize pairing]. The following conclusions could be obtained if we agree that $\beta_8 < 0$ situation is realized in reality.

(1) For a reasonable weight of coefficient β_8 (for example, $-0.5 < \mathrm{sign}(\beta_8)\beta_8^2 < 0$) the population for the $[s^2_{1/2}]$ state in ^{10}He is expected to be larger than for the $[p^2_{1/2}]$ state ($\sigma_{10}/\sigma_8 \sim$ 0.9–3.5).
(2) Population cross section for the ^{10}He $[p^2_{1/2}]$ state cannot differ strongly from that obtained for the ^{8}He g.s. For the realistic structure of ^{6}He the values lying in a range of $\sigma_{10}/\sigma_8 \sim$ 0.6–1.3 are expected.
(3) Population rate for the 3 MeV group of events in ^{10}He is found consistent with the resonant cross section estimated for the population of the p-wave state. Coefficient β_8 can be obtained from the experimentally measured cross sections for the pop-

ulation of ^{8}He and ^{10}He ground states: $\beta_8^2 \approx 0.1^{+0.3}_{-0.1}$. In this work such a derivation is methodologically clean as both cross sections are obtained in the same experimental conditions.

(4) Note that the model proposed here (with neutrons situated only in the p-shell) shows that the basic dynamics of the ^{8}He system strongly limits the possible range of the ^{6}He g.s. configuration weight in the ^{8}He structure [see Fig. 4(a)]. This implies that the weights corresponding to the ^{6}He g.s. and ^{6}He(2^+) configurations in the structure of ^{8}He have only a weak dependence on the $[p^4_{3/2}]_0$ and $[p^2_{3/2}p^2_{1/2}]_0$ configuration mixing.

(5) The spectroscopic factor for processes with the disintegration of ^{8}He in ^{6}He(g.s.) + $2n$ continuum is connected with the weight in Eq. (3) by relation

$$S_8^{2n} = 6\left\|\langle\Psi^0_{^8\mathrm{He}}|\Psi^0_{^6\mathrm{He}}\rangle\right\|.$$

A discrepancy can be seen in Ref. [22] between the experimentally obtained $S_8^{2n} = 1.3(1)$ and theoretical "shell model" value given as 1/6 (see Table 1 in [22]). The S_8^{2n} values obtained in our model vary between 0.8 and 1.1 (depending on the β_8 value) in a good agreement with the experiment of Ref. [22].

6. Possible nature of the threshold state in ^{8}He

In the missing mass spectrum of ^{8}He (see Fig. 2) attention is attracted by a steep rise ensuing straight from the three-body $^6\mathrm{He} + n + n$ threshold. The lowest known resonant state of ^{8}He is 2^+ at $E = 3.57$ MeV [14], $\Gamma = 0.5$–0.7 MeV. It decays sequentially via the ^{7}He ground state resonance ($3/2^-$ at $E_{^7\mathrm{He}} = 0.445$ MeV, $\Gamma = 0.15$ MeV) by a p-wave neutron emission. This guarantees the negligible population of the continuum below ~ 0.6 MeV where the decay takes place in a "three-body regime", $\sigma \sim E^4_{^8\mathrm{He}}$. Above that energy, the population probability transfers to the "two-body p-wave regime", $\sigma \sim E^{3/2}_{^8\mathrm{He}}$. Consequently, the low-energy tail of the 2^+ state cannot be responsible for the near threshold events.

The only plausible source of the low-energy events, we have found, is the population of the E1 (means 1^-) continuum. The theoretical studies of such a continuum populated in reactions [23–25] show that the profile of the 1^- cross section typically well resembles the profile of the electromagnetic strength function dB_{E1}/dE. Such functions for spatially extended halo systems could provide a very low-energy peak – the so-called soft dipole mode – even without the formation of any 1^- resonant state.

We estimate the E1 strength function for the $^8\mathrm{He} \to ^6\mathrm{He} + 2n$ dissociation using the model developed in [26]. For the WF with outgoing asymptotic

$$\Psi_E^{(+)}(\mathbf{X},\mathbf{Y}) = \int d\mathbf{X}'\, d\mathbf{Y}'\, G_E^{(+)}(\mathbf{X}\mathbf{X}', \mathbf{Y}\mathbf{Y}')\hat{D}\Psi_{\mathrm{g.s.}}(\mathbf{X},\mathbf{Y}) \tag{4}$$

generated by the dipole operator $\hat{D}$, acting on the g.s. WF $\Psi_{\mathrm{g.s.}}$, the E1 strength function is found as

$$\frac{dB_{\mathrm{E1}}}{dE} = \frac{2J_f+1}{2J_i+1}\frac{X^2}{2\pi}\,\mathrm{Im}\left[\int d\Omega_x \int d\mathbf{Y}\,\Psi_E^{(+)\dagger}\frac{\nabla_x}{M_x}\Psi_E^{(+)}\right]\Bigg|_{X\to\infty}.$$

Vectors $\mathbf{X}$ and $\mathbf{Y}$ are the Jacobi coordinates for the ^{6}He–n and (^{6}He–n)–n subsystems, respectively. Estimating the dipole strength for the light p-shell nuclei we can well take into account only the $[p^2] \to [sp]$ transitions and neglect the nn interactions and s-wave interaction between the core and neutron (unless the latter is not strongly attractive). In this approximation the three-body Green's function (GF) has a simple analytical form

$$G_E^{(+)}(\mathbf{X}\mathbf{X}', \mathbf{Y}\mathbf{Y}') = \frac{1}{2\pi i}\int dE_{^7\mathrm{He}}\, G^{(+)}_{E_{^7\mathrm{He}}}(\mathbf{X},\mathbf{X}')G^{(+)}_{E-E_{^7\mathrm{He}}}(\mathbf{Y},\mathbf{Y}'),$$

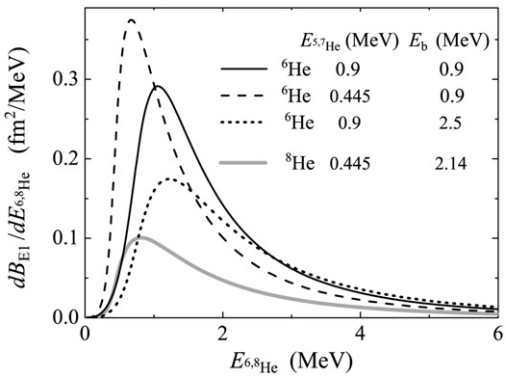

Fig. 5. E1 strength function for ^{6}He and ^{8}He. The dashed and dotted curves show calculations done for ^{6}He with unrealistic parameters demonstrating the trends in the strength functions behaviour with the parameter variation.

where $G^{(+)}_{E-E_{^7\mathrm{He}}}$ is a free motion GF in the Y subsystem, and the GF in the X subsystem corresponds to the p-wave continuum with the ^{7}He g.s. $3/2^-$ resonance at $E_{^7\mathrm{He}} = 0.445$ MeV.

The results of the model calculations, including the ^{6}He test, are shown in Fig. 5. The estimated ^{6}He strength function giving a peak at about 1.1 MeV is in a reasonable agreement with the complete three-body calculations [23] giving the peak at about 1.3 MeV. It can be seen that the strength function profile in ^{6}He is sensitive to the following two main aspects of the dynamics.

(i) Energy of the resonance ground state in the p-wave subsystem: dashed curve shows that the strength function peak is shifting to the *lower* energy if the ^{5}He $3/2^-$ state is artificially shifted from the experimental $E_{^5\mathrm{He}} = 0.9$ MeV position to the *lower* 0.445 MeV.

(ii) "Size" of the ground state WF: dotted curve shows the strength function peak shifting to *higher* energy if we artificially overbound the ^{6}He g.s. WF to $E_b = 2.5$ MeV instead of 0.9 MeV *decreasing* its radial extent.

When we turn from ^{6}He to ^{8}He these dynamical trends work in the opposite directions and largely compensate each other (the ^{8}He g.s. is more "compact" than the ^{6}He g.s., but the ^{7}He g.s. resonance is lower than the ^{5}He g.s. resonance). As a result we find the strength function peak position in ^{8}He to be somewhat lower than the respective position in ^{6}He. This indicates that in ^{8}He, where the 2^+ state is significantly higher than in ^{6}He, the lowest-energy feature in the continuum could be the 1^- excitation.

The behaviour of the cross section with the estimated E1 component taken into account is shown in Fig. 6. The 2^+ state profile is given here by the standard R-matrix expression for the p-wave decay via the ^{7}He g.s. providing the widths $\Gamma = 0.56$–0.82 MeV for excitation energies $E = 3.6$–3.9 MeV (the reduced width is taken as the Wigner limit). Without the E1 contribution the data are in agreement with the standard position ($E \approx 3.6$ MeV) of the 2^+ state, but the near threshold behaviour of the cross section cannot be reproduced. The 2^+ population cross section in this case can be estimated as ~ 250 μb/sr. The addition of the 1^- contribution allows to reproduce the low-energy part of the spectrum much better. In that case we can allow up to 60% feeding to the 1^- continuum. Then we get ~ 100 μb/sr for the 2^+ population and have to shift to about $E \approx 3.9$ MeV the position of this state.

The proposed significant contribution of the 1^- cross section is not an absolutely unexpected and never seen phenomenon. For example, the experimental spectrum from paper [27] is shown in the inset to Fig. 6. Inspected around the $^6\mathrm{He} + n + n$ threshold "on a large scale" it shows the same presence of the low-energy intensity

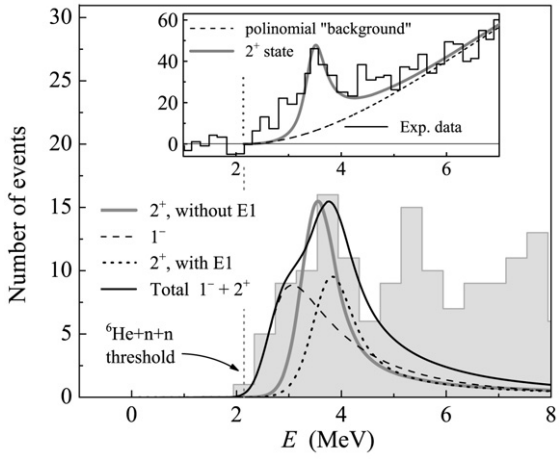

Fig. 6. Experimental spectrum of Fig. 2 is compared to the theoretical profile of the 2^+ state with and without a possible contribution of the 1^- continuum. The theoretical curves are convoluted with the experimental resolution. The experimental data of [27] are shown in the inset. Dashed curve is the result of a polynomial "background" subtraction and solid gray line is the same as the solid gray line in the main panel (convoluted with the experimental resolution of [27]).

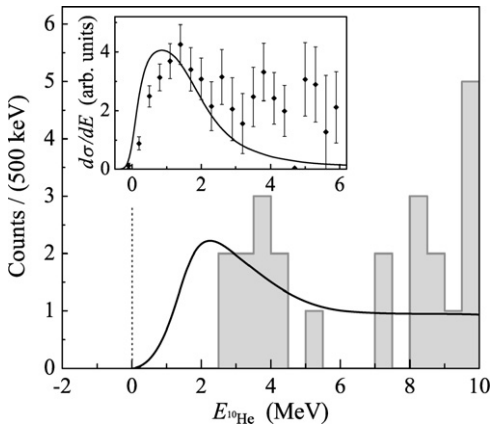

Fig. 7. Missing mass spectrum of ^{10}He compared to the predictions of Ref. [11] for the ^{10}He g.s. with the $[p^2_{1/2}]$ structure. The inset shows the experimental data of Ref. [4] compared to the theoretical spectrum obtained with the same Hamiltonian as in the main panel but for the different reaction mechanism.

which cannot be attributed to the left "wing" of the 2^+ resonant state. The strong population of the E1 continuum in ^{8}He by nuclear processes has been demonstrated in a comparison made for the nuclear and Coulomb dissociation data [28,29]. However, in the interpretation of the data presented in [28,29] the idea was accepted that the E1 cross section in ^{8}He should peak at *higher* energy than in ^{6}He (maximum at about $E_{^8\mathrm{He}} \approx 2$ MeV above the threshold). This idea is based on the argument (ii) discussed above (smaller size of ^{8}He compared to ^{6}He); the actual situation appears to be more complicated. As a result the authors of [28,29] have had to position the 2^+ state *below* the E1 peak. Consequently, they had to ascribe to it a very low excitation energy 2.9 MeV (compared to about 3.6 MeV in the other recent works). The assumption of the very low-energy soft E1 peak in ^{8}He would probably allow to explain the data from [28,29] in a more natural way. Also, there exists a large uncertainty in the definition of the "standard" position of the 2^+ state in ^{8}He (2.7–3.6 MeV, see Ref. [15]). We think that a significant component of the disagreement among different experimental works could be connected with the possibility that the 2^+ state is typically observed in a mixture with the 1^- contribution. Correlation measurements could clarify this situation.

7. Interpretation of the ^{10}He spectrum

There is an evident discrepancy between the group of events at about 3 MeV observed in this experiment and the recognized position of ^{10}He g.s. at about 1.2 MeV. Basing on the ^{8}He experimental data, the estimated cross section for population of the 0^+ state in ^{10}He is *more* than 120 μb/sr in *any considered model case* (see Section 5). This means that over 8 events should be expected below 2.5 MeV in the ^{10}He spectrum. The absence of events below 2.5 MeV has a large statistical significance, despite the low statistics of the spectrum itself. The observation of none events in that energy range due to pure statistical reasons has probability less than $e^{-8} \sim 3 \times 10^{-4}$ (the Poisson distribution is assumed). A possible explanation is that an excited state of ^{10}He was observed in our work and the ground state was not populated for some reason: the 3 MeV group of events is consistent, in principle, with the position of the first excited state of ^{10}He (~ 4.3 MeV) found in Ref. [5]. This explanation requires that our cross section estimates are wrong: the reaction mechanisms with ^{6}He and ^{8}He beams should be not analogous in reality or/and the assumptions about the structure of helium isotopes underlying the estimates of Section 5 should be not true. We find a different explanation preferable.

There are two important problems, pointed by theoreticians, in the interpretation of the ^{10}He spectrum.

(i) A possible existence of a near-threshold 0^+ state with the $[s^2_{1/2}]$ structure, due to the shell inversion phenomenon [9]. In this case we would have two 0^+ states in the low-energy continuum of ^{10}He, nearby each other. The $[s^2_{1/2}]$ state is predicted in [11] to have very specific properties (tentatively assigned as "three-body virtual state") and it distorts strongly the higher-lying spectrum associated with the $[p^2_{1/2}]$ 0^+ state. At a first glance it is not impossible that the $[s^2_{1/2}]$ 0^+ state is not populated in our experiment.

(ii) The reaction mechanism issue was pointed in Ref. [11]. The most clear observation of the ^{10}He g.s. was made so far in the experiment with the ^{11}Li beam [4]. It was shown in [11] that, in contrast to the typical transfer reactions, the experiments with the ^{11}Li beam can provide very specific signal for the $[p^2_{1/2}]$ 0^+ state: in the ^{11}Li case the spectrum is shifted downwards due to the abnormal size of the halo component of the ^{11}Li WF.

We, therefore, need to provide explanation to the two problems: (i) nonobservation of the 0^+ state with the $[s^2_{1/2}]$ structure and (ii) nonobservation of the 0^+ state with the $[p^2_{1/2}]$ structure below 2.5 MeV.

Let us consider the second issue first. The measured missing mass spectrum of ^{10}He is shown in Fig. 7 in comparison with the experimental data [4] and calculations [11] taking into account the reaction mechanisms in both cases. It is clear that the calculations are somewhat overbound (~ 0.5–0.7 MeV), but otherwise consistent with the data in both cases. It has also been shown in Section 5 that the absolute cross section value for the 3 MeV group of events is quantitatively consistent with the population of a p-wave state. We can conclude here that it is very probable that the 1.2 MeV peak observed in Ref. [4] and the 3 MeV peak in our work represent the same state. It should be emphasized that the calculated peak energy for the (t, p) reaction cross section is consistent with the resonance properties inferred from the S-matrix in [11]: the eigenphase for $3 \to 3$ scattering is passing $\pi/2$ at about the peak energy. Therefore, the peak energy observed in the transfer reaction could provide a better access to the ^{10}He properties.

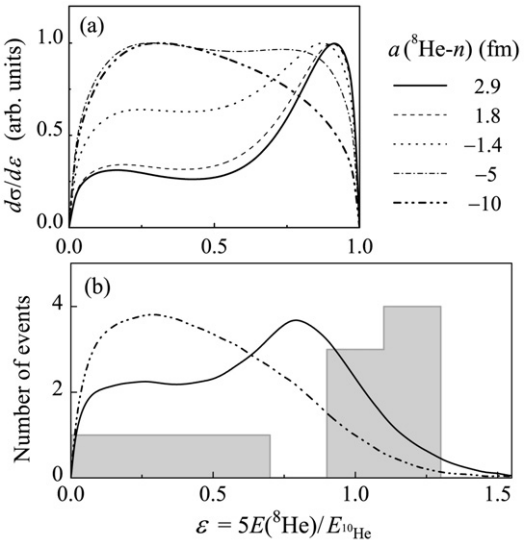

Fig. 8. Energy distribution of ^{8}He in the ^{10}He CMS frame. (a) Calculated in Ref. [11] for different interactions in the ^{8}He–n channel. The corresponding scattering lengths are shown in the legend; positive a values correspond to repulsive interactions. Solid curve corresponds to the theoretical missing mass spectrum given in Fig. 7 (^{10}He g.s. with $[p^2_{1/2}]$ structure). (b) $E(^8\mathrm{He})$ distribution observed in the present work for the 3 MeV group of events is shown as a gray histogram. Theoretical curves are the same as in panel (a) convoluted by the MC procedure with the experimental resolution.

Now we return to the first issue. Is it possible that the theoretically predicted in Ref. [9] low-lying 0^+ state with the $[s^2_{1/2}]$ structure exists, but it is not populated in our reaction? It was shown in [11] that the expected 0^+ states with the $[s^2_{1/2}]$ and $[p^2_{1/2}]$ structures would interfere strongly. The momentum distributions for the $[p^2_{1/2}]$ state were predicted to be strongly different in the cases when there *is* an $[s^2_{1/2}]$ state below it and when there *is no* such state. This point is illustrated in Fig. 8(a) for different interactions in the ^{8}He–n s-wave channel (the positive values of scattering length indicated for two curves in Fig. 8(a) imply that a repulsive interaction takes place in the s-wave state). In Ref. [11] the cases of $a < -5$ fm in ^{9}He correspond to the formation of extremely sharp near threshold 0^+ ^{10}He states. Otherwise, there is only the $[p^2_{1/2}]$ state at ~ 2.4 in the ^{10}He continuum. It can be seen in Fig. 8(b) that only scattering lengths $a \geqslant -5$ fm (and hence no $[s^2_{1/2}]$ state) are qualitatively consistent with our data. Thus the data favour the situation of the $[p^2_{1/2}]$ ground state of ^{10}He. In this way our data also indirectly lead to a contradiction with the ^{8}He–n scattering length limit $a < -10$ fm claimed in Ref. [8].

The interpretation proposed above is very nonorthodox and is based, at the moment, on the limited statistics data. However, it provides a consistent explanation of all features of the system observed so far. Alternatively, we face a problem to explain why the "real" ground state was not observed in our experiment despite the very low cross section limit achieved ($\sigma_{10} < 14$ μb/sr) and the estimates of Section 5 indicating large population probability.

8. Conclusion

In this work we studied the ^{8}He and ^{10}He spectra in the same (t, p) transfer reaction. This allowed us to avoid the treatment of the reaction mechanism peculiarities. We think that in the sense of the data our results are not in contradiction with the previous works done on these nuclei. However, making various theoretical estimates we arrived at different conclusions on several issues.

The ground 0^+ and the excited 2^+, (1^+) states of ^{8}He are populated with cross sections 200, $\sim$ 100–250, and $\sim$ 90–125 μb/sr. The presence of near-threshold events at about $E \sim 2.14$ MeV can be evidence for the formation of the soft dipole mode in the ^{8}He continuum. The generation of such a mode with the very low peak energy ($E_{^8\mathrm{He}} \sim 0.9$ MeV, $E \sim 3$ MeV) in nuclear reactions could possibly be an explanation to the respective controversial features of the other ^{8}He data as well.

We have considered the nonobservation of events corresponding to the expected ^{10}He g.s. below 2.5 MeV to be a serious problem. A possible explanation to this problem can be found in Ref. [11]. According to the calculations of Ref. [11] the 3 MeV peak position obtained here for the ^{10}He g.s. is in agreement with the 1.2 MeV position found in Ref. [4], if one takes into account the peculiar reaction mechanism for the ^{11}Li beam used in [4]. If this interpretation is valid, a new ground state energy of about 3 MeV should be established for ^{10}He since the peak position obtained in the transfer reaction corresponds to the S-matrix pole position, while for the reactions with ^{11}Li there is a strong difference.

It should be noted that the population cross section of the 3 MeV peak in ^{10}He $\sigma_{10} = 140(30)$ μb/sr is consistent with the estimated resonance cross section for the population of the ^{10}He 0^+ state with the $[p^2_{1/2}]$ structure. If this is accepted, the weight $\beta_8 \approx 0.1^{+0.3}_{-0.1}$ of the $[p^2_{3/2}p^2_{1/2}]$ configuration in ^{8}He can be inferred from the σ_{10}/σ_8 ratio.

The absence of the near-threshold state in ^{10}He predicted to have an $[s^2_{1/2}]$ structure [9] imposes, according to calculations [11], a stringent limit $a \geqslant -5$ fm on the ^{8}He–n scattering length. This is in contradiction with the existence of a virtual state in ^{9}He declared to have $a < -10$ fm in Ref. [8].

Further measurements of a similar style are desirable. These would allow to finally resolve the intriguing issues outlined in this work.

Acknowledgements

We are grateful to Profs. B.V. Danilin, S.N. Ershov, V.Z. Goldberg, and M.V. Zhukov for illuminating discussions. The authors acknowledge the financial support from the INTAS Grants Nos. 03-51-4496 and 05-100000-8272, Russian RFBR Grants Nos. 05-02-16404, 08-02-00089 and 05-02-17535 and Russian Ministry of Industry and Science grant NS-1885.2003.2. Support provided for this work by the Department of Science and Technology of South Africa is acknowledged.

References

[1] A.A. Yukhimchuk, et al., Nucl. Instrum. Methods A 439 (2003) 513.
[2] M.S. Golovkov, et al., Phys. Rev. Lett. 93 (2004) 262501.
[3] M.S. Golovkov, et al., Phys. Rev. C 72 (2005) 064612.
[4] A.A. Korsheninnikov, et al., Phys. Lett. B 326 (1994) 31.
[5] A.N. Ostrowski, et al., Phys. Lett. B 338 (1994) 13.
[6] H.G. Bohlen, et al., Prog. Part. Nucl. Phys. 42 (1999) 17.
[7] A.A. Korsheninnikov, B.V. Danilin, M.V. Zhukov, Nucl. Phys. A 559 (1993) 208.
[8] L. Chen, et al., Phys. Lett. B 505 (2001) 21.
[9] S. Aoyama, Phys. Rev. Lett. 89 (2002) 052501.
[10] M.S. Golovkov, et al., Phys. Rev. C 76 (2007) 021605, (R).
[11] L.V. Grigorenko, M.V. Zhukov, Phys. Rev. C 77 (2008) 034611.
[12] A.M. Rodin, et al., Nucl. Instrum. Methods A 391 (1997) 228.
[13] I. Tilquin, et al., Nucl. Instrum. Methods A 365 (1995) 446.
[14] A.A. Korsheninnikov, et al., Phys. Lett. B 316 (1993) 38.
[15] D.R. Tilley, et al., Nucl. Phys. A 745 (2004) 155.
[16] F. Skaza, et al., Nucl. Phys. A 788 (2007) 260c.
[17] S.C. Pieper, R.B. Wiringa, J. Carlson, Phys. Rev. C 70 (2004) 054325.
[18] V.P. Pandharipande, Nucl. Phys. A 738 (2004) 66.
[19] A. Volya, V. Zelevinsky, Phys. Rev. Lett. 94 (2005) 052501.
[20] M.V. Zhukov, A.A. Korsheninnikov, M.H. Smedberg, Phys. Rev. C 50 (1994) R1.

[21] B.V. Danilin, et al., Phys. Rev. C 43 (1991) 2835.
[22] L.V. Chulkov, et al., Nucl. Phys. A 759 (2005) 43.
[23] B.V. Danilin, et al., Nucl. Phys. A 632 (1998) 383.
[24] S.N. Ershov, B.V. Danilin, J.S. Vaagen, Phys. Rev. C 64 (2001) 054608.
[25] S.N. Ershov, et al., Phys. Rev. C 70 (2004) 054608.
[26] L.V. Grigorenko, K. Langanke, N.B. Shul'gina, M.V. Zhukov, Phys. Lett. B 641 (2006) 254.
[27] H.G. Bohlen, et al., in: Proceedings of LEND'95, World Scientific, 1995, p. 53.
[28] K. Markenroth, et al., Nucl. Phys. A 679 (2001) 462.
[29] M. Meister, et al., Nucl. Phys. A 700 (2002) 3.